

Microstructure and Wear Performance of ECAP Processed Cast Al–Zn–Mg Alloys

G. K. Manjunath¹ · K. Udaya Bhat¹ · G. V. Preetham Kumar¹ · M. R. Ramesh²

Received: 28 February 2018 / Accepted: 9 April 2018 / Published online: 9 May 2018
© The Indian Institute of Metals - IIM 2018

Abstract In the present investigation, wear performance of equal channel angular pressing (ECAP) processed cast Al–Zn–Mg alloys under dry sliding wear conditions was studied against a steel disc. Initially, Al–Zn–Mg alloys (with 5, 10, 15% zinc and 2% magnesium) were ECAP processed. After ECAP, grain size was reduced and enhancement in the hardness was observed. Wear resistance of the alloys increased after ECAP processing. Wear resistance of the alloys also increased when the quantity of the zinc was increased in the alloys. But, wear resistance of all three alloys decreased with increase in the load and the sliding speed. Coefficient of friction of the alloys decreased after ECAP processing. Coefficient of friction of the alloys also decreased when the quantity of the zinc was increased in the alloys. Coefficient of friction of all three alloys increased with increase in the load and the sliding speed. Irrespective of the alloy composition and applied load,

worn surfaces of the cast and homogenized samples were composed of plastic deformation, scratches and micro-ploughing. On the other hand, in ECAP processed samples, morphology of the worn surfaces depended on the applied load. Abrasive wear is the main wear mechanism perceived in cast and homogenized samples at all loads. While in ECAP processed samples, the wear mechanism shifted from adhesive and oxidation wear to abrasive wear with increase in the load. Formation of oxide layers on the surface of the sample increased with increase in the ECAP passes. In ECAP processed samples, transfer of iron content from the disc to the sample surface was identified.

Keywords Al–Zn–Mg alloy · ECAP · Wear · Coefficient of friction · Wear mechanism

1 Introduction

Aluminium and its alloys are superior substitutes for other metallic materials in structural, transport and industrial applications owing to its higher specific strength. Amongst all aluminium alloys, Al–Zn–Mg alloys are recognised as the strongest and hardest aluminium alloys [1]. In recent years, heat treatable Al–Zn–Mg alloys have gained massive attention as the major materials in aerospace and automotive industries [1]. Al–Zn–Mg alloys possess good tensile properties, dimensional stability, machinability and recommended for service at elevated temperatures [2]. However, low strength and poor ductility of Al–Zn–Mg alloy in cast condition limits its application in engineering applications. In addition, aluminium alloys show poor wear properties in cast condition [3]. Wear properties have major effect on the durability and serviceability of engineering appliances [3]. Wear is an important parameter to be

Electronic supplementary material The online version of this article (<https://doi.org/10.1007/s12666-018-1328-6>) contains supplementary material, which is available to authorized users.

✉ K. Udaya Bhat
udayabhatk@gmail.com
G. K. Manjunath
manjugk2001@gmail.com
G. V. Preetham Kumar
pkphd@hotmail.com
M. R. Ramesh
ramesdmt@gmail.com

¹ Department of Metallurgical and Materials Engineering, National Institute of Technology Karnataka, Surathkal, Mangalore 575025, India

² Department of Mechanical Engineering, National Institute of Technology Karnataka, Surathkal, Mangalore 575025, India

considered in design and development of engineering components and there is an enormous interest to improve wear resistance through various techniques and one of them is through strengthening methods [4].

Amongst, various strengthening methods (to improve the strength and the wear resistance of the material) strengthening through grain refinement method is more attractive because of its simplicity [5]. Grain refinement can be achieved through severe plastic deformation (SPD) methods. In SPD methods, higher level of grain refinement and high degree of misorientation between the grains can be achieved [6]. Also, ultrafine grained (UFG) materials obtained through SPD methods exhibits superior mechanical properties [6]. At present, several SPD techniques are available and the most efficient and auspicious technique is equal channel angular pressing (ECAP) [7]. Segal et al. [8] were the first to introduce the ECAP process in 1981. This process has now become the successful technique compared to other SPD methods. In ECAP process, the deformation takes place by pure shear. The principle of ECAP is that, a sample of uniform cross-section is pressed through a set of channels having identical cross-sections, meeting at an angle (Φ). Large amount of shear strain is developed in the sample as it passes the plane of intersection between two channels. The cross-section of the sample remains constant at both entrance and exit channels, large plastic strain can be accomplished by processing the sample repeatedly [9].

UFG materials processed by SPD methods possess higher hardness, higher strength and good ductility compared to coarse grained (CG) materials. UFG materials are anticipated to possess adequate wear resistance [3]. Also, in order to make optimum use of materials processed by SPD, it is very essential to study their wear properties. However, in spite of enormous studies on their mechanical properties [10], superplasticity [11] and other topics [12, 13], wear properties of ECAP processed Al–Zn–Mg alloys have not received much attention. There have been merely few literatures reported on the wear properties of the ECAP and other SPD processed materials. La et al. [14] reported that due to increased hardness and strength after ECAP processing, wear rate decreased in commercially pure titanium. Wang et al. [15] reported that due to loss of strain hardening capability during ECAP processing, wear resistance decreased in Al 1050 alloy. Ibrahim et al. reported that wear resistance capability of Al–Cu alloy enhanced with increase in the number of ECAP passes [16]. Kucukomeroglu [17] reported that even though the strength of the material enhanced after ECAP processing; the wear resistance decreased in ECAP processed Al–12Si alloy. Gao and Cheng [4] reported that grain refinement and enhancement in the hardness obtained during ECAP enhanced the wear resistance and load bearing capacity of

Cu–10Al–4Fe alloy. Kim et al. [18] reported that due to cracking at the interface between the martensite and the ferrite matrix, wear resistance decreased in ECAP processed low carbon Fe–0.15C dual phase steel. Purcek et al. [19] reported that wear resistance of the ECAP processed Zn–40Al–2Cu–Si material increased due to the enhancement in the toughness and ductility of the material after ECAP processing. Kim et al. [18] reported that in spite of possessing higher strength and hardness, accumulative roll bonding (ARB) processed Al 5052 alloy possessed low wear resistance due to low strain-hardening capability.

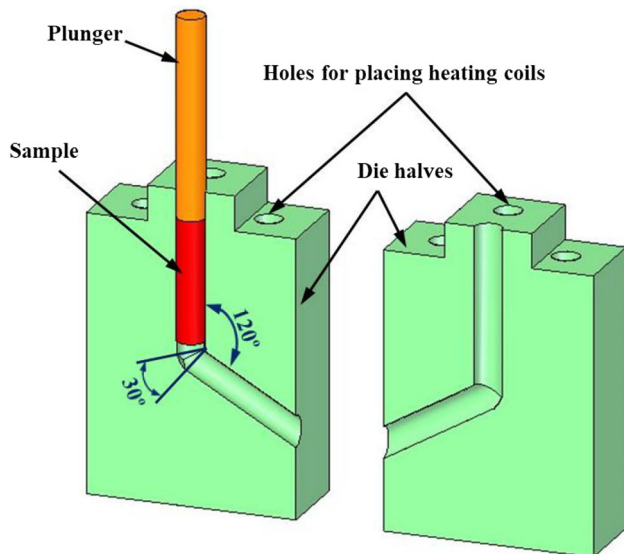
From the literature, contradictory results (both favourable and unfavourable effects) were observed in the wear properties of ECAP and other SPD processed materials. This might have been attributed to the various factors like wear mechanisms, presence of precipitates and strain hardening. The present study is motivated by the realization that, until now no scientific investigations have been carried out on the wear performance of the ECAP processed cast Al–Zn–Mg alloys with varying zinc content. So it is interesting to study the effect of ECAP processing on the wear performance of cast Al–Zn–Mg alloys. In the present work, Al–Zn–Mg alloys (5, 10, 15% zinc and 2% magnesium) were ECAP processed. The effect of zinc content and the ECAP passes on the wear performance have been investigated.

2 Experimental Procedure

The alloys used in the present study are shown in Table 1. The alloys were prepared by gravity casting method. The details of sample preparation through gravity casting method were available in earlier report [20]. After casting, alloys were homogenized for 20 h at 480 °C. For ECAP processing, samples of \varnothing 16 mm and 85 mm length were machined. Three dimensional view of the ECAP die with plunger and sample is shown in Fig. 1. The ECAP die has $\Phi = 120^\circ$ and $\Psi = 30^\circ$. From these angles, 0.667 strain is developed in each pass. In the present work, route B_C was adopted. It resulted in uniform distribution of the strain in the material compared to other routes [21]. ECAP processing was carried out at 200 °C. This was the minimum temperature at which all three alloys were successfully processed, up to four passes in route B_C without failure. After four passes, processing was stopped, since in route B_C distortion reinstated the equiaxed microstructure in all three planes after every four successive passes [21]. The ECAP processing was carried out at a speed of 0.5 mm/s in a universal testing machine. Molybdenum disulphide (MoS₂) was used as the lubricant to avoid the friction between the die and the specimen. Heating coils were used to heat the ECAP die assembly to the required processing

Table 1 Chemical compositions of the alloy (in wt%) used in the study

Alloy	Abbreviation	Aluminium	Zinc	Magnesium
Al–5Zn–2Mg	A5	93	5	2
Al–10Zn–2Mg	A10	88	10	2
Al–15Zn–2Mg	A15	83	15	2

**Fig. 1** Model of the ECAP die

temperature and the particular temperature was retained throughout the processing.

Microstructure of the specimens was captured by using JEOL JSM 6380LA scanning electron microscope (SEM) operating at 20 kV. For microstructural analysis, unprocessed and processed samples were cut perpendicular to the processing direction, followed by polishing through metallographic techniques and finally etched with Keller's etchant. Grain size measurements were carried out through linear interception method using Image J software. Microhardness measurements were carried out according to ASTM E384 standard using Shimadzu Vickers hardness machine (model: HMV-G20 ST) by applying 50 g load up to 15 s. In all specimens, 10 hardness measurements were carried out and average values were considered.

Wear test experiments were carried out in a pin on disc type test setup according to ASTM G-99 standard. Wear test experiments were carried out in DUCOM pin on disc equipment (model: TR-20LE-PHM 400-CHM 600). The wear test experiments were conducted at ambient temperature and at a relative humidity of $55 \pm 5\%$. Specimens for the wear test experiments were machined to $\varnothing 10$ mm and 28 mm in length cylindrical pins. Prior to each test, sample surfaces were polished with 1200 grit size silicon carbide

emery paper ($0.3 \mu\text{m}$ roughness was maintained) and cleaned with acetone. Samples were made to slide against EN31 (E52100) steel disc (hardness: 62 HRC and surface roughness: $0.3 \mu\text{m}$). The composition of the EN31 steel is presented in Table 2. Before wear test, the disc surface was polished with silicon carbide (600 grit) abrasive paper and cleaned with acetone. During wear test, sliding of the samples followed a circular path of 120 mm track diameter. To identify the influence of load on the material loss, two different loads of 20 N and 40 N were applied. Also, to identify the influence of sliding speed on the material loss, wear test experiments were carried out at two different sliding speeds, namely, 1 and 2 m/s. In all cases, wear test experiments were carried out for a fixed distance of 1000 m. Mass loss technique was used to measure the wear damage. Microbalance (accuracy ± 0.01 mg) was used for this purpose. The coefficient of friction ($\mu = F_f/P$) values were calculated by using frictional force data recorded in the computer and the applied load [22]. Three specimens were tested in each condition and the average values were considered. The surface morphology and the energy dispersive spectroscopy (EDS) study of the worn surfaces of the wear test specimens were carried out by using SEM.

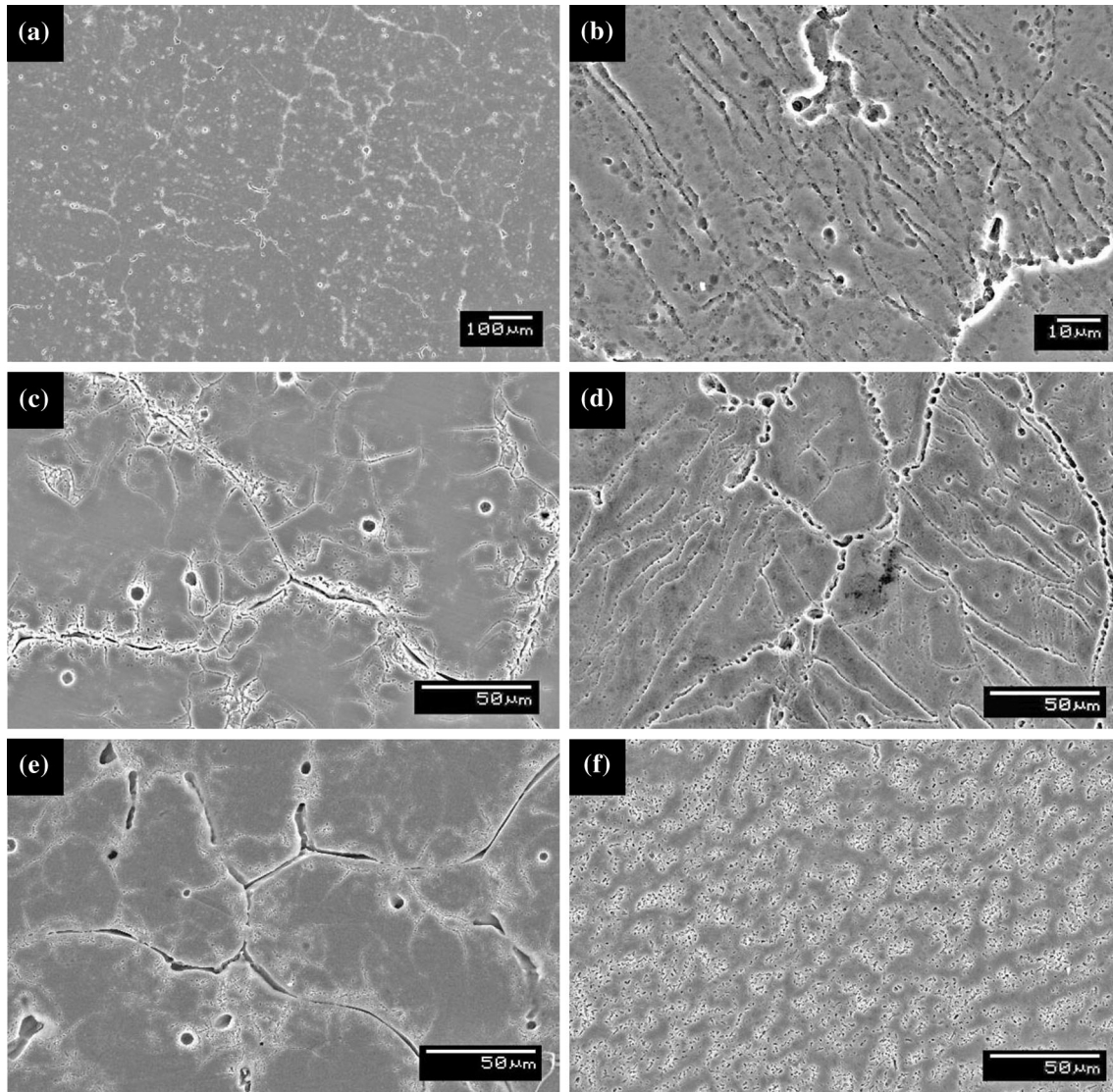
3 Results and Discussion

3.1 Microstructural Evolution

SEM micrograph of the A5 alloy in cast form is presented in Fig. 2a. In this condition, large sized dendrites and secondary particles are identified in the dendrites. The secondary particles are noticed as η' phase (MgZn_2) precipitates [23]. Dendrites of size $200 \pm 20 \mu\text{m}$ are observed in cast condition. After homogenization treatment, grains of size $180 \pm 20 \mu\text{m}$ are observed. Noticeable grain refinement is observed after ECAP processing. The crystallite size reduces to 30 ± 10 , 20 ± 8 , 10 ± 6 and $5 \pm 3 \mu\text{m}$ in first, second, third and fourth passes, respectively [24]. Figure 2b shows the SEM micrograph of the A5 alloy after four ECAP passes in route B_C. SEM micrograph of the A10 alloy in cast form is presented in Fig. 2c. Under this condition, large sized dendrites and secondary particles are identified in the dendrites. The

Table 2 Chemical compositions (in wt%) of the EN31 steel

Element	C	Si	Mn	Cr	P	S	Mo	Fe
Weight%	0.95–1.1	0.1–0.35	0.25–0.4	1.2–1.6	0.04	0.05	0.06	Balance

**Fig. 2** Microstructure of the **a** A5 alloy in cast condition, **b** A5 alloy after 4 pass, **c** A10 alloy in cast condition, **d** A10 alloy after 4 pass, **e** A15 alloy in cast condition and **f** A15 alloy after 4 pass

secondary particles are noticed as η' phase (MgZn_2) precipitates. Dendrites of size $280 \pm 40 \mu\text{m}$ are observed in cast condition. After homogenization treatment, grains of size $260 \pm 20 \mu\text{m}$ are observed. Significant grain refinement is observed after ECAP processing. The crystallite size reduces to 75 ± 10 , 40 ± 8 , 20 ± 7 and $8 \pm 5 \mu\text{m}$ in first, second, third and fourth passes, respectively [24]. Figure 2d shows the SEM micrograph of the A10 alloy after four ECAP passes in route B_C. SEM micrograph of

the A15 alloy in cast form is shown in Fig. 2e. In this condition, large sized dendrites and secondary particles are identified in the dendrites. The secondary particles are noticed as η' phase (MgZn_2) precipitates. Dendrites of size $200 \pm 20 \mu\text{m}$ are observed in cast condition. After homogenization treatment, grains of size $180 \pm 18 \mu\text{m}$ are obtained. Substantial grain refinement is observed after ECAP processing. The crystallite size reduces to 50 ± 15 , 25 ± 10 , 15 ± 5 and $10 \pm 5 \mu\text{m}$ in first, second, third and

fourth passes, respectively [24]. Figure 2f shows the SEM micrograph of the A15 alloy after four ECAP passes in route B_C. It is noticed that, MgZn₂ precipitate formation in the material increases when the zinc quantity in the material is increased. During ECAP processing, the hard secondary particles get sheared and evenly distributed in the aluminium matrix [25].

3.2 Hardness

Figure 3 shows the changes in the hardness with ECAP passes for different alloy composition. In cast condition, hardness of the A5 alloy is 90 ± 8 Hv. After homogenization treatment, hardness increases to 105 ± 6 Hv. Noticeable enhancement in the hardness is observed after ECAP processing. The hardness of the A5 alloy increases to 158 ± 6, 175 ± 6, 184 ± 4 and 188 ± 4 Hv in first, second, third and fourth passes, respectively. In cast condition, hardness of the A10 alloy is 144 ± 8 Hv. After homogenization treatment, hardness increases to 155 ± 6 Hv. Significant enhancement in the hardness can be perceived after ECAP processing. The hardness of the A10 alloy increases to 204 ± 6, 223 ± 5, 232 ± 5 and 240 ± 4 Hv in first, second, third and fourth passes, respectively. In cast condition, hardness of the A15 alloy is 173 ± 7 Hv. After homogenization treatment, hardness increases to 189 ± 6 Hv. Substantial enhancement in the hardness can be observed after ECAP processing. The hardness of the A15 alloy increases to 239 ± 6, 261 ± 6 Hv in the first and second passes, respectively. After third pass, hardness of the A15 alloy increases to 274 ± 5 Hv. After fourth pass, hardness does not increase and remains constant.

After four passes, the hardness is enhanced by 109, 67 and 58% in A5, A10 and A15 alloys, respectively from the

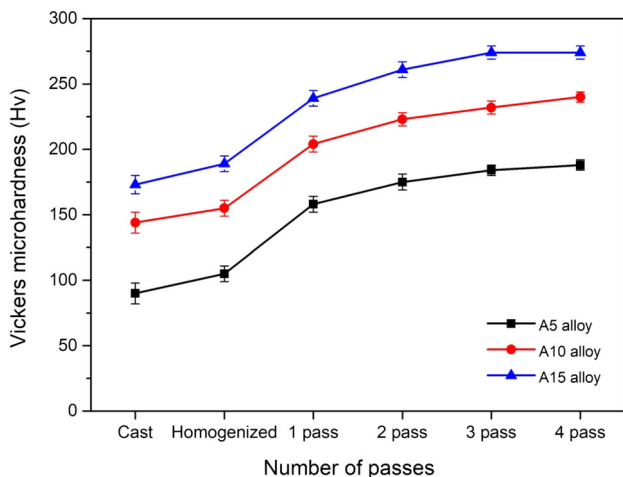


Fig. 3 Variation of the hardness with number of ECAP passes and alloy composition

initial condition [24]. The enhancement in the hardness after ECAP processing is attributed to the reduced grain size, work hardening, high dislocation density, precipitates which is finely fragmented and evenly distributed in the material [25]. Also, hardness of the material increases when the zinc quantity in the material is increased. This is attributed to the fact that increased zinc content increases MgZn₂ precipitate formation. Consequently, hardness of the material increases with increase in the MgZn₂ precipitate in the material.

3.3 Wear Characteristics

Figure 4a displays the wear mass loss of A5 alloy under various conditions. It can be perceived that, for the same load and the sliding speed, ECAP processed samples exhibit higher wear resistance than the unprocessed sample. Wear resistance of the alloy enhances with increase in the ECAP passes. At 20 N load and 1 m/s sliding speed, the mass loss in cast condition is 7.4 mg and it reduces to 2.8 mg after four ECAP passes. Also, for the same condition of the sample, the mass loss is increased with increment in the applied load and the sliding speed. At 20 N load and 1 m/s sliding speed, the mass loss in homogenized condition is 6.5 mg and it increases to 11.8 mg at 40 N load and 2 m/s sliding speed. Compared to the increase in the sliding speed, increase in the load has more pronounced effect on the mass loss of the material. This is supported by the following observation. At 20 N load and 1 m/s sliding speed the mass loss in the sample subjected to four ECAP pass is 2.8 mg and it increases to 5.8 mg at 40 N load and 1 m/s sliding speed, while at 20 N load and 2 m/s sliding speed, the mass loss is only 4 mg. The improvement in the wear resisting capability of the material after ECAP processing is consistent with earlier observations on cast Zn–40Al–2Cu–2Si alloy processed by ECAP [19]. Improvement in the wear resisting capability of the material after ECAP processing is attributed to the reduced grain size and enhancement in the hardness of the material during ECAP processing. This is related to Archard’s relation [26]:

$$V = K \frac{LF}{H} \tag{1}$$

where *K* is the wear coefficient related to ductility of the material, *L* is the total sliding distance, *F* is the load applied, *H* is the hardness of the specimen and *V* is the wear loss in volume. According to Archard’s equation, for materials with sufficient ductility, wear is inversely proportionate to the strength and hardness of the material. Generally, cast materials are brittle in nature and for brittle materials; the *K* value is higher leading to reduction in the

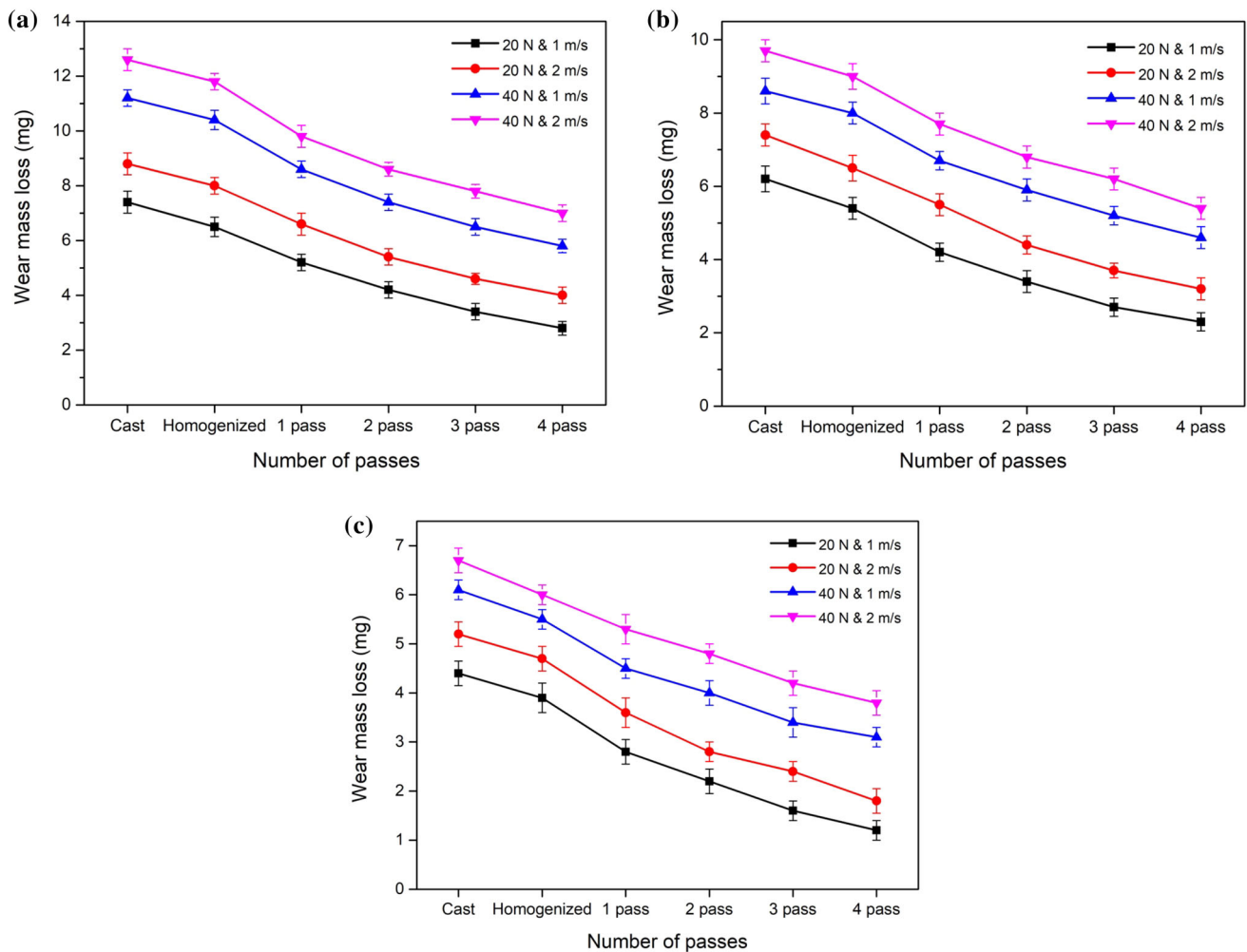


Fig. 4 Wear mass loss of **a** A5 alloy in various conditions, **b** A10 alloy in various conditions, **c** A15 alloy in various conditions

wear resistance. It can be observed that, processing by ECAP has positive effect on the wear properties. Amongst all cases, wear mass loss is highest in cast condition and lowest in four ECAP pass sample which is attributed to the smallest grain size observed after four ECAP passes.

Figure 4b, c displays the wear mass loss of A10 and A15 alloy, respectively in various conditions. In both the alloys, similar to A5 alloy, the behaviour of enhancement in the wear resistance with increase in the ECAP passes can be observed. It is noted that for the same the load and the sliding speed, A10 alloy possesses better wear resistance than A5 alloy. At 20 N load and 2 m/s sliding speed, the mass loss of A5 alloy in cast condition is 8.8 mg, while for the same load and sliding speed, the mass loss of A10 alloy in cast condition is reduced to 7.4 mg. Similarly, for the same load and the sliding speed, A15 alloy possess better wear resistance than A5 and A10 alloy. At 20 N load and 2 m/s sliding speed, the mass loss of A15 alloy in cast condition is 5.2 mg. The increase in the wear resistance of A10 alloy compared to A5 alloy and increase in wear

resistance of A15 alloy compared to A5 and A10 alloy is attributed to increased zinc content. Increase in the zinc content lead to increase in the quantity of $MgZn_2$ precipitates in the material. When $MgZn_2$ precipitate formation in the material increases, hardness of the material also increases. Hence, it can be deduced that, both the increase in the zinc quantity in the material and ECAP processing contribute to the increased wear resistance in A10 and A15 alloy.

Figure 5a shows the coefficient of friction (μ) of A5 alloy in various conditions. It is observed that, the coefficient of friction of ECAP processed samples is lower than the cast and homogenized samples. Also, coefficient of friction reduces with increase in the ECAP passes. For the same condition of the sample, the coefficient of friction is enhanced with increase in the applied load and the sliding speed. In all cases, the coefficient of friction is highest in cast condition and lowest in four ECAP pass samples. At 20 N load and 1 m/s sliding speed, the coefficient of friction in cast condition is 0.42 and it reduces to 0.3 after four

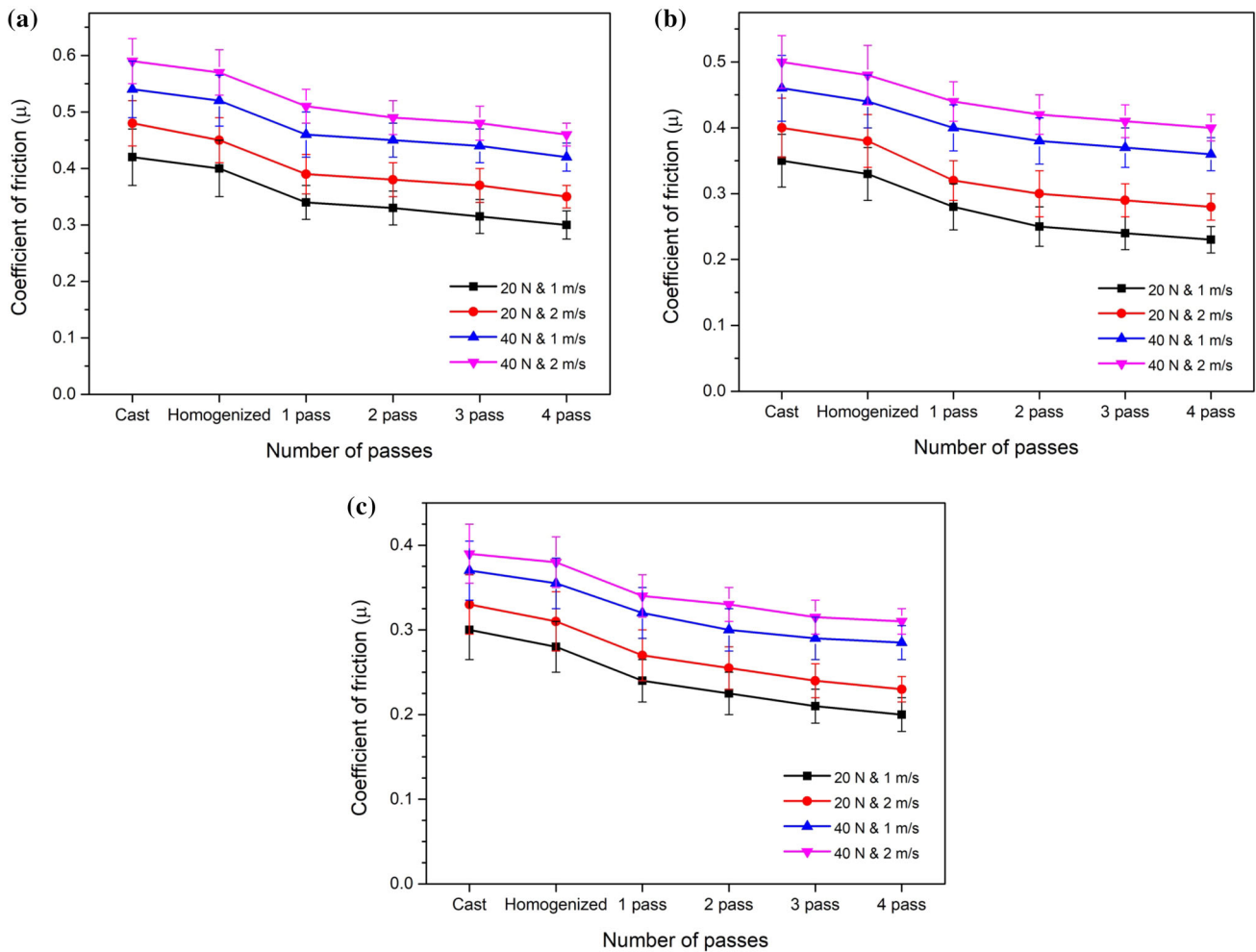


Fig. 5 Coefficient of friction of **a** A5 alloy in various conditions, **b** A10 alloy in various conditions, **c** A15 alloy in various conditions

ECAP passes. At 40 N load and 2 m/s speed, the coefficient of friction in cast condition is 0.59 and it reduces to 0.46 after four ECAP passes. Even though, the coefficient of friction reduces after ECAP processing, close examination reveals that the variation coefficient of friction ranges in between 0.3 and 0.59. The decrease in coefficient of friction after ECAP processing is owing to the decrease in the grain size and enhancement in the hardness of the material. The reduction in the coefficient of friction with ECAP processing is consistent with earlier observations on Cu–10Al–4Fe alloy processed by ECAP [4].

Figure 5b, c shows the coefficient of friction of A10 and A15 alloy, respectively, in various conditions. Similar to A5 alloy, in both the alloys, the behaviour of reduction in coefficient of friction with increase in the ECAP passes can be observed. It is noted that for the same the load and the speed, A10 alloy possesses low coefficient of friction than A5 alloy. Similarly, for the same load and the speed, A15 alloy possesses low coefficient of friction than A5 and A10 alloy. In A10 alloy, the lowest coefficient of friction

observed is 0.23 and highest coefficient of friction observed is 0.5. In A15 alloy, the lowest coefficient of friction observed is 0.39. In all three alloys, thorough examination reveals that fluctuation in coefficient of friction is more in cast samples and fluctuation get reduced with increase in the ECAP passes. This is attributed to nonhomogeneous cast structure initially, which get refined and become homogenous microstructure during ECAP processing.

3.4 Analysis of the Worn Surfaces and the Wear Mechanisms

Figure 6 shows the SEM micrographs of the worn surfaces after wear tests, carried out at load 20 N and at 1 m/s sliding speed for A5 alloy in various conditions. Figure 6a shows the worn surface of the material in cast condition; micrograph indicates brittle type of wear damage. In the sliding direction, scratches and micro-ploughing grooves are observed. Scratches and ploughing grooves on the worn

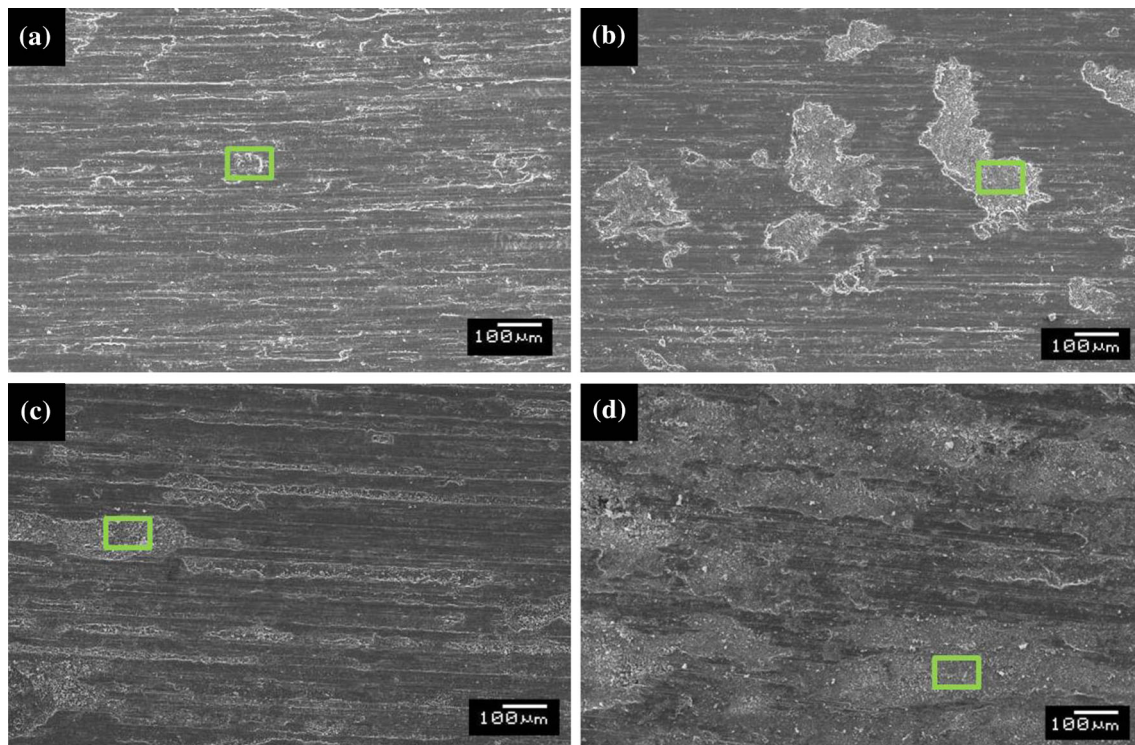


Fig. 6 SEM micrographs of the worn surfaces after wear test under a load of 20 N and at speed of 1 m/s of A5 alloy **a** cast, **b** 1 pass, **c** 2 pass and **d** 4 pass. From the marked regions EDS data is collected and shown in Fig. 7

surfaces are attributed to abrasive action of the hard secondary particles which are separated from the sample and get entrapped between the mating surfaces. The abrasive action is of three body abrasive wear. Similar to cast sample, scratches, delamination and ploughing in the sliding direction are observed in the homogenized sample. Thus, it can be deduced that the wear mechanism involved in the cast sample and homogenized samples are abrasive wear. Figure 6b shows the worn surface of the ECAP sample after first pass, along with scratches, delamination and ploughing in the sliding direction; smearing and adhering of the worn debris are also observed. The wear debris of the ECAP processed sample is adhered to the mating surfaces rather than separating from the mating surfaces. This is attributed to the enhancement in the deformability after ECAP processing [19]. Therefore, both abrasive and adhesive wear mechanism is perceived in first ECAP pass sample. With increase in the ECAP passes, smearing and adhering of the worn debris to the surface of the sample increases as shown in Fig. 6c, d. Consequently, scratches and delamination on the worn surfaces are reduced with increase in the ECAP passes. Thus, with increase in the ECAP passes, abrasive wear mechanism is replaced with adhesive wear mechanism. It is noted that, the effectiveness of smearing and adhesion of wear debris is more in four pass sample compared to one pass and two pass samples.

Figure 7 shows the EDS analysis of the worn surfaces after wear tests, carried out at load 20 N and at 1 m/s sliding speed for A5 alloy in various conditions. Aluminium possesses high tendency towards oxidation. This characteristics of aluminium plays a vital character in wear behaviour of the alloy. Figure 7a shows the EDS analysis of the cast sample. Even though a small trace of oxygen can be observed, its effect in the formation of any oxide layers is not observed in SEM micrograph. Since, the hardness of the cast sample is less compared to ECAP processed samples, the load applied is sufficient to remove the oxide layer which leads to metal to metal contact, causing increase in the wear rate. Consequently in cast sample, the oxidation effect is not observed. Therefore, under cast condition, abrasive wear is the leading wear mechanism. Figure 7b–d shows the EDS analysis of the worn surfaces of the first pass, second pass and four ECAP pass samples. In all 3 samples, presence of oxygen is observed in adhered debris. The presence of oxygen proves the formation of oxide layers on the sample surface. Since, the hardness of the ECAP processed samples is higher than the unprocessed samples, the load applied is not sufficient to remove the oxide layer which causes decrease in wear rate. Consequently wear rate is very less in ECAP processed samples. Therefore, along with adhesive wear; oxidation wear is also involved in ECAP processed samples. Decrease in wear rate due to the presence of oxidation

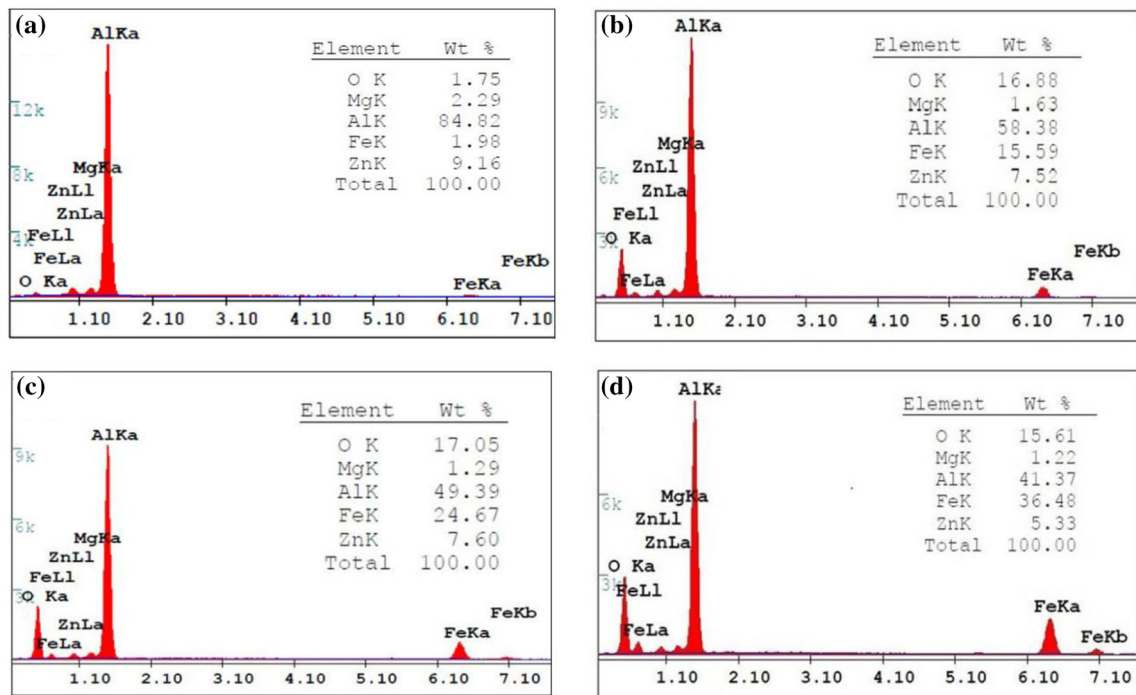


Fig. 7 EDS analysis of the worn surfaces after wear test under a load of 20 N and at sliding speed of 1 m/s of A5 alloy **a** cast, **b** 1 pass, **c** 2 pass and **d** 4 pass. EDS data is collected from the marked region indicated in Fig. 6

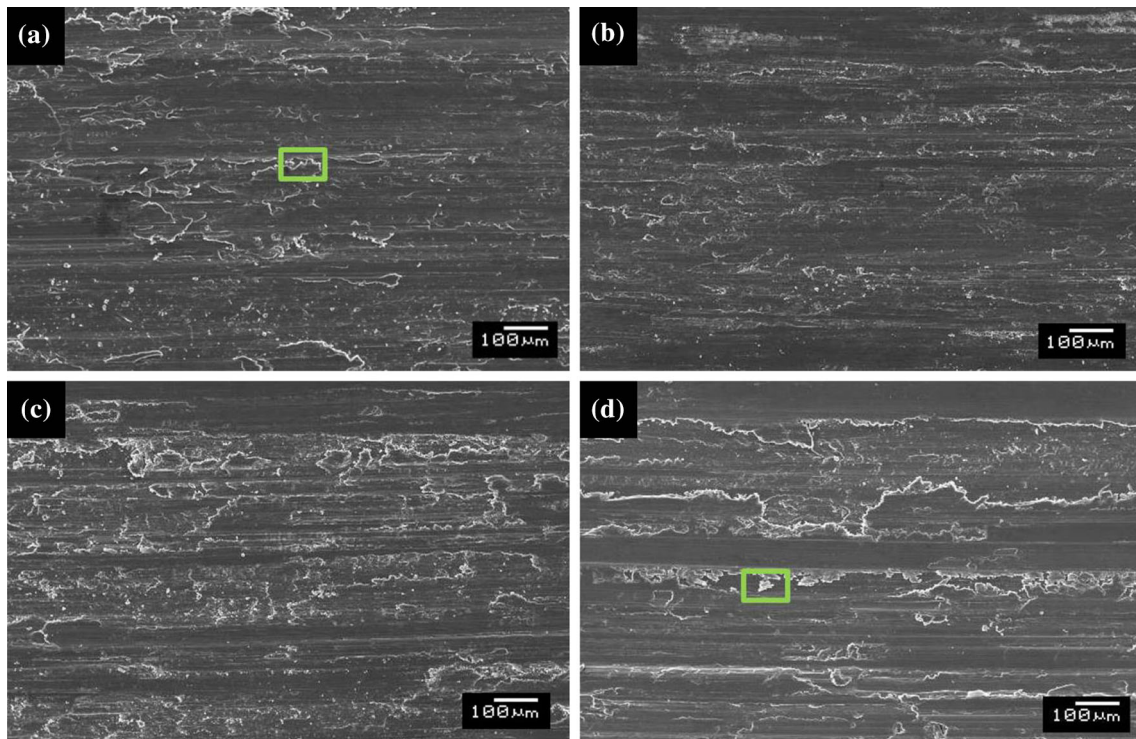


Fig. 8 SEM micrographs of the worn surfaces after wear test under a load of 40 N and at speed of 2 m/s of A5 alloy **a** cast, **b** 1 pass, **c** 2 pass and **d** 4 pass. From the marked regions EDS data is collected and shown in Fig. 9

wear in ECAP processed samples is consistent with earlier observations on ECAP processed AZ31 magnesium alloy

[27]. Also in the EDS analysis, the existence of Fe can be observed. The existence of Fe confirms the movement of

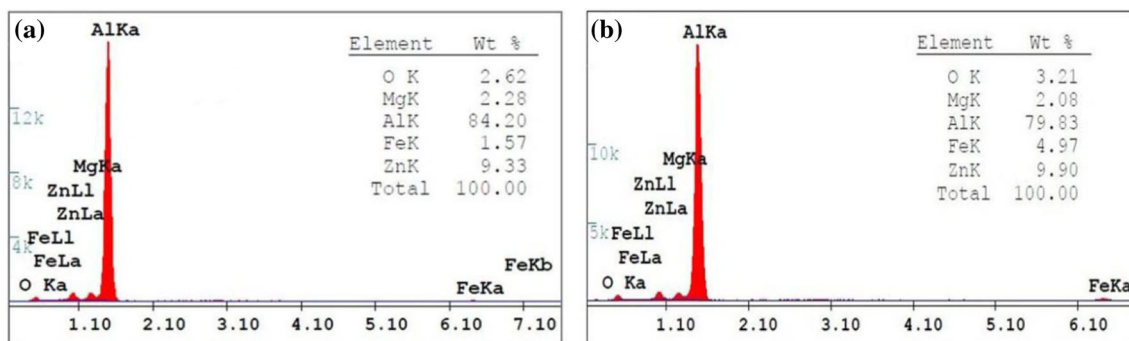


Fig. 9 EDS analysis of the worn surfaces after wear test under a load of 40 N and at sliding speed of 2 m/s of A5 alloy **a** cast and **b** 4 pass. EDS data is collected from the regions marked in Fig. 8

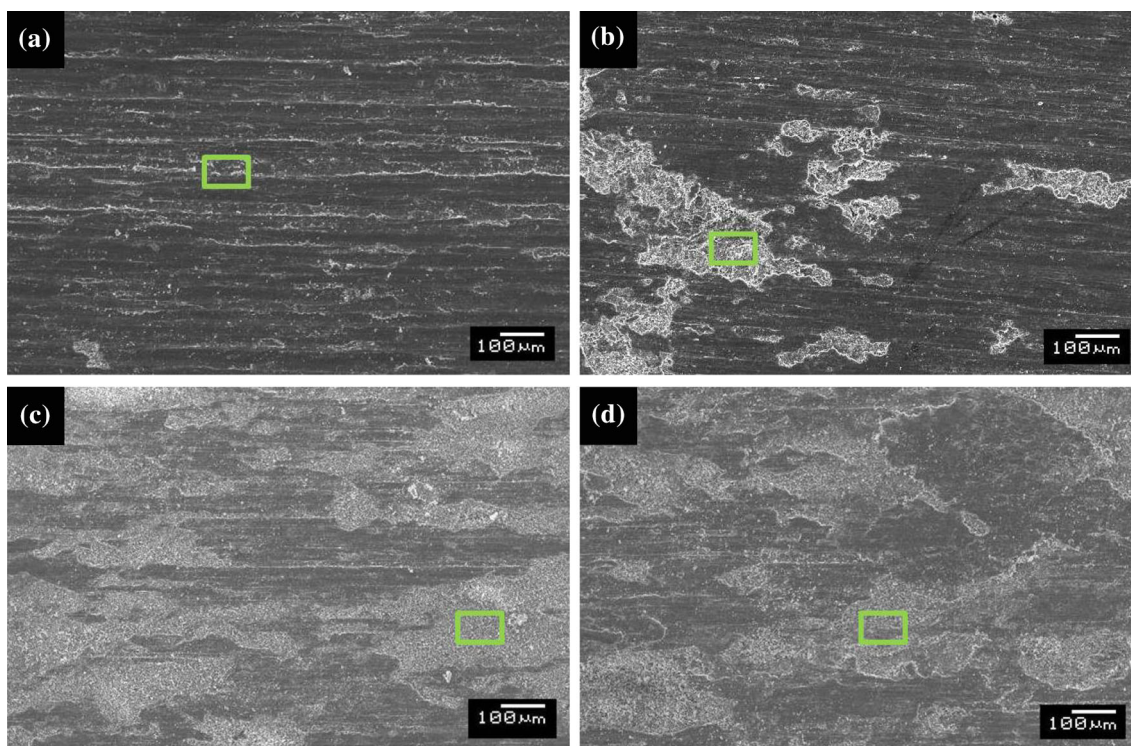


Fig. 10 SEM micrographs of the worn surfaces after wear test under a load of 20 N and at speed of 1 m/s of A15 alloy **a** cast, **b** 1 pass, **c** 2 pass and **d** 4 pass. EDS data is collected from the marked regions and are given in Fig. 11

the Fe particles from the disc to the sample surface. The movement of the Fe particles from disc to the sample is attributed to the enhancement in hardness of the sample after ECAP processing. It may be noted that, movement of the Fe particles from the disc to the sample surface increases with subsequent ECAP passes. Also, the formation of oxide layer increases with subsequent ECAP passes. Thus, oxidation wear mechanism is more in four pass sample compared to one pass and two pass samples. The movement of the Fe particles from disc to the sample is consistent with earlier observations on ECAP processed cast Al–Cu alloy [16].

Figure 8 shows the SEM micrographs of the worn surfaces after wear tests, carried out at load 40 N and at 2 m/s sliding speed for A5 alloy in various conditions. In this condition, severe wear features are perceived compared to wear features perceived at 20 N load and 1 m/s sliding speed. Worn surfaces exhibits high plastic deformation characterized by wide and deep ploughing grooves. In the sliding direction, delamination is observed in cast samples, as shown in Fig. 8a. In ECAP processed samples, the severity of wear get reduced compared to cast sample, as shown in Fig. 8b–d. This is due to increase in hardness of the alloy after ECAP processing. In this condition, smearing and adhering of the worn debris is not observed

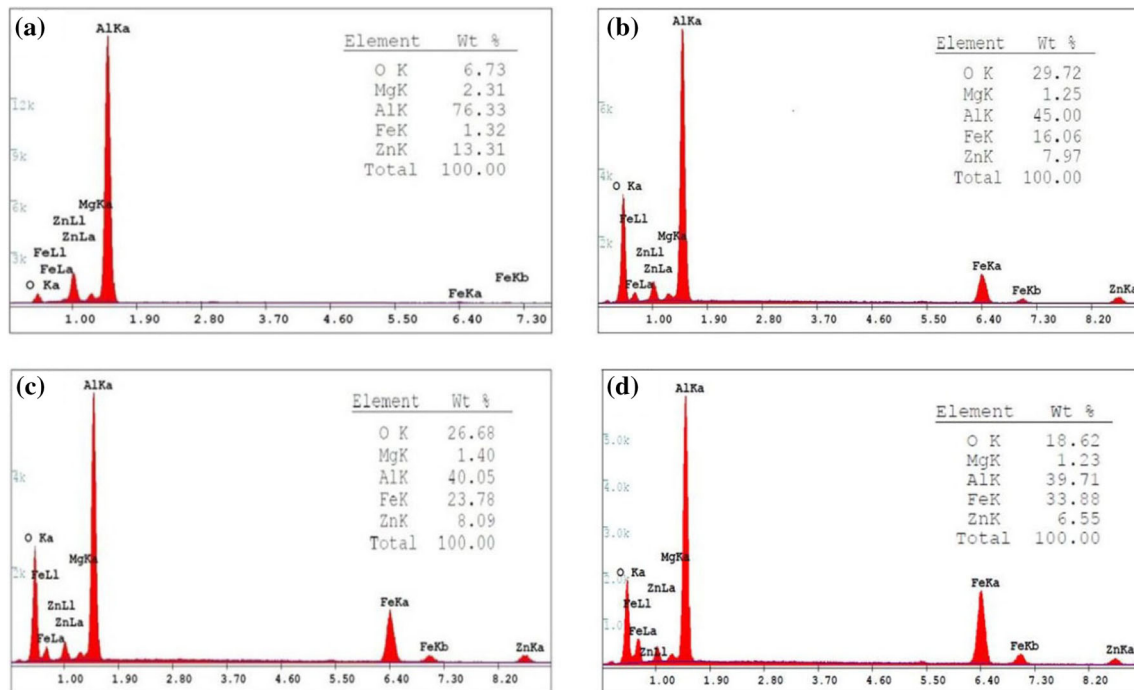


Fig. 11 EDS analysis of the worn surfaces after wear test under a load of 20 N and at sliding speed of 1 m/s of A15 alloy **a** cast, **b** 1 pass, **c** 2 pass and **d** 4 pass. EDS locations are marked in Fig. 10

in ECAP processed samples. Since, under this condition, the load applied and sliding speed is more, the worn debris might have left the sliding surfaces. Therefore, in this case, abrasive wear is the leading mechanism observed in both the processed and unprocessed samples. Figure 9 shows the EDS analysis of the worn surfaces after wear tests, carried out at load 40 N and at 2 m/s sliding speed of A5 alloy in cast condition and after four ECAP passes. Even though a few traces of oxygen is observed in the EDS analysis of the cast condition and four ECAP passes, its effect on oxide layer formation can not be observed in SEM micrographs. In this case, the load applied and the sliding speed is more which remove the oxide layer leading to metal to metal contact which causes increase in wear rate. The traces of Fe observed is comparatively less in this condition when compared to 20 N load and 1 m/s sliding speed. This may be due to the fact that at higher load and at higher sliding speed, Fe particles might have left the sliding surface. So, it is deduced that abrasive wear is the prevailing mechanism for both the processed and unprocessed samples in this condition.

Figure 10 shows the SEM micrographs of the worn surfaces after wear tests, carried out at load 20 N and at 1 m/s sliding speed for A15 alloy under various conditions. Figure 10a presents the SEM micrograph of the sample in cast condition. The worn morphologies are identical to those morphologies perceived in A5 alloy for the same load and sliding speed conditions. In cast sample, the worn

surface consists of scratches and delamination due to spalling of sample particles in the form of debris, which results in abrasive wear. Figure 10b shows the worn surface of the first ECAP pass sample. Here, along with scratches, delamination and ploughing in the direction of sliding, smearing and adhering of the worn debris are also observed. Both abrasive and adhesive wear mechanism are observed in first ECAP pass sample. Figure 10c, d displays the worn surface of the second and four ECAP pass samples, respectively. It is observed that, the effectiveness of smearing and adhesion of debris is maximum in four ECAP pass sample and minimum in first ECAP pass sample. Subsequently, material delamination and micro-ploughing grooves on the worn surfaces are reduced with increase in the ECAP passes. Hence, adhesive wear is the prevailing wear mechanism in the ECAP processed samples. Figure 11 shows the EDS analysis of the worn surfaces after wear tests, carried out at load 20 N and at 1 m/s sliding speed for A15 alloy in various conditions. Figure 11a shows the EDS analysis of the cast sample. Along with large traces of aluminium and zinc, negligible traces of Fe and oxygen are observed. Figure 11b–d shows the EDS analysis of the worn surfaces of the first pass, second pass and four ECAP pass samples, respectively. In the EDS analysis of the ECAP processed samples, existence of oxygen and Fe are observed in debris adhered to the sample surfaces. This behaviour is similar to A5 alloy (for the same load and sliding speed). Therefore, both adhesive

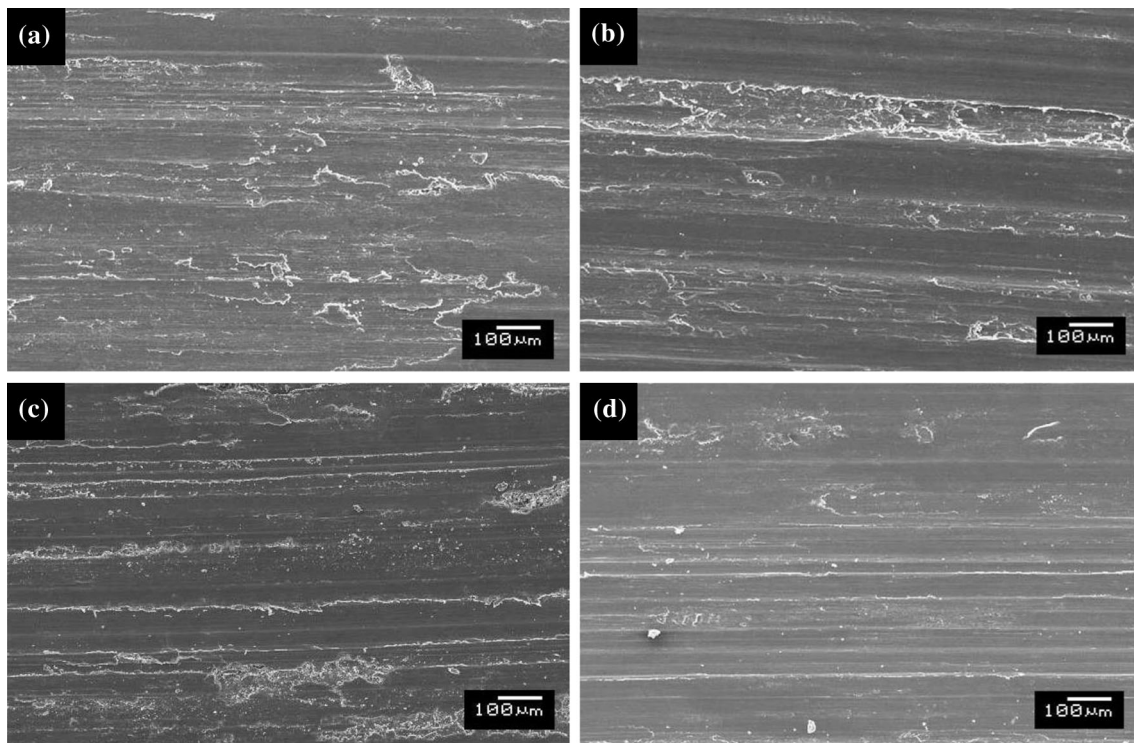


Fig. 12 SEM micrographs of the worn surfaces after wear test under a load of 40 N and at speed of 2 m/s of A15 alloy **a** cast, **b** 1 pass, **c** 2 pass and **d** 4 pass

wear and oxidation wear is involved in ECAP processed samples. It is noted that, similar to A5 alloy, the movement of the Fe particles from the disc to the sample surface and formation of oxide layer in the sample surface, both increases with subsequent ECAP passes.

Figure 12 shows the SEM micrographs of the worn surfaces after wear tests, carried out at load 40 N and at 2 m/s sliding speed for A15 alloy under various conditions. The worn surface morphologies are almost identical to those perceived in A5 alloy (at load 40 N and sliding speed 2 m/s). Scratches and delamination of material can be observed on the worn surfaces of the cast sample as shown in Fig. 12a. This indicates the presence of abrasive wear. Even though the scratches and material delamination are observed on the worn surface of the ECAP processed samples as shown in Fig. 12b–d, but the intensity of wear is less compared to cast sample. Wear crater is observed in some areas of first ECAP pass sample as shown in Fig. 12b. In four ECAP pass sample, relatively smooth surface morphology is observed as shown in Fig. 12d. The intensity of wear decreases with increase in the ECAP passes. Under this condition, smearing and adhering of the worn debris is not observed in ECAP processed samples. This behaviour is similar to A5 alloy (for the same load and sliding speed). This indicates that, all samples undergo abrasive wear mechanism under this condition. It is noted that, compared to ECAP processed A5 alloy, the worn

surfaces of ECAP processed A15 alloy are less damaged (at load 40 N and sliding speed 2 m/s). This may be credited to increased hardness and strength of ECAP processed A15 alloy compared to ECAP processed A5 alloy.

4 Conclusions

In the present investigation, wear properties of cast Al–Zn–Mg alloys (with 5, 10 and 15% zinc and 2% magnesium) processed by ECAP in route B_C up to 4 number of passes at 200 °C was studied. The outcomes of the work are as follows:

- After ECAP processing, large reduction in the grain size of the material and considerable improvement in the hardness of the material was witnessed.
- In all three alloys, wear resistance capability of the material was increased after ECAP processing. Also, wear resistance of the material was enhanced with increase in the zinc quantity in the alloy. In all three alloys, wear resistance capability of the material was reduced with increase in the load and the sliding speed. Compared to the increase in the sliding speed, increase in the load had more pronounced impact on wear resistance. In all conditions, highest wear resistance

was observed in A15 alloy compared to other two alloys.

- In all three alloys, coefficient of friction was reduced with increase in the ECAP passes due to reduction in the grain size after ECAP processing. Also, coefficient of friction was reduced when zinc quantity was increased in the material. In all three alloys, coefficient of friction increased with increase in the load and sliding speed.
- In cast and homogenized samples, both at lower and higher load; material delamination, scratches and micro-ploughing grooves were observed on the worn surfaces. While in the ECAP processed samples, only at higher load material delamination, scratches and micro-ploughing grooves were observed on the worn surfaces, at lower load, smearing and adhering of wear debris was observed on the worn surfaces.
- In cast samples, abrasive wear mechanism was observed both in lower and higher load. While in ECAP processed samples, adhesive wear mechanism and oxidation wear mechanism was witnessed in lower load and it was replaced by abrasive wear mechanism with increase in the load. In ECAP processed samples, at lower load, movement of the Fe particles from disc to sample surface was observed. Also, movement of the Fe particles from disc to sample surface increased with subsequent ECAP passes.

References

1. Shaeri M H, Salehi M T, Seyyedain S H, Abutalebi M R, and Park J K, *Mater Des* **57** (2014) 250.
2. Kutz M, *Mechanical Engineers Handbook: Materials and Mechanical Design*, Wiley, New Jersey (2006).
3. Gao N, Wang C T, Wood R J K, and Langdon T G, *J Mater Sci* **47** (2012) 4779.
4. Gao L L and Cheng X H, *Wear* **265** (2008) 986.
5. Valiev R Z, Estrin Y, Horita Z, Langdon T G, Zehetbauer M J, and Zhu Y T, *JOM* **58** (2006) 33.
6. Valiev R Z, Islamgaliev R K, and Alexandrov I V, *Prog Mater Sci* **45** (2000) 103.
7. Valiev R Z and Langdon T G, *Prog Mater Sci* **51** (2006) 881.
8. Segal V M, Raznikov V I, Drobyshevsky A E, and Kopylov V I, *Russ Metall* **1** (1981) 99.
9. Zehetbauer T and Zhu M J, *Bulk Nanostructured Materials*, Wiley-VCH, Weinheim (2009).
10. Kumar S R, Gudimetla K, Venkatachalam P, Ravisankar B, and Jayasankar K, *Mater Sci Eng A* **533** (2012) 50.
11. Xu C, Furukawa M, Horita Z, and Langdon T G, *Acta Mater* **51** (2003) 6139.
12. Xu C and Langdon T G, *Mater Sci Eng A* **410** (2005) 398.
13. Shaeri M H, Shaeri M, Salehi M T, Seyyedain S H, and Djavaanroodi F, *Trans Nonferrous Met Soc China* **25** (2015) 1367.
14. La P, Ma J, Zhu Y T, Yang J, Liu W, Xue Q, and Valiev R Z, *Acta Mater* **53** (2005) 5167.
15. Wang C T, Gao N, Wood R J K, and Langdon T G, *J Mater Sci* **46** (2011) 123.
16. Ibrahim M I A E, Mahallawy N E, Shehata F A, Hameed M A E, Yoon E Y, and Kim H S, *Mater Sci Eng A* **527** (2010) 3726.
17. Kucukomeroglu T, *Mater Des* **31** (2010) 782.
18. Kim Y S, Yu H S, and Shin D H, *Int J Mat Res* **100** (2009) 871.
19. Purcek G, Saray O, Kucukomeroglu T, Haouaoui M, and Karaman I, *Mater Sci Eng A* **527** (2010) 3480.
20. Manjunath G K, Preetham Kumar G V, and Udaya Bhat K, *Trans Indian Inst Met* **70** (2017) 833.
21. Furukawa M, Iwahashi Y, Horita Z, Nemoto M, and Langdon T G, *Mater Sci En A* **257** (1998) 328.
22. Wang Z B, Tao N R, Li S, Wang W, Liu G, Lu J, and Lu K, *Mater Sc Eng A* **352** (2003) 144.
23. Zhang S, Hu W, Berghammer R, and Gottstein G, *Acta Mater* **58** (2010) 6695.
24. Manjunath G K, Udaya Bhat K, and Preetham Kumar G V, *Metallogr Microstruct Anal* **7** (2018) 77.
25. Zheng L J, Li H X, Hashmi M F, Chen C Q, Zhang Y, and Zeng M G, *J Mater Process Technol* **171** (2006) 100.
26. Archard J F, *J. Appl Phys* **24** (1953) 981.
27. Xu J, Wang X, Zhu X, Shirooyeh M, Wongsan-Ngam J, Shan D, Guo B, and Langdon T G, *J Mater Sci* **48** (2013) 4117.